THE JOURNAL OF PHYSICAL CHEMISTRY C

Article

pubs.acs.org/JPCC

Interaction between Olivine and Water Based on Density Functional Theory Calculations

Valentina Prigiobbe,*[,†] Ana Suarez Negreira,[‡] and Jennifer Wilcox[§]

[†]Department of Petroleum and Geosystems Engineering, The University of Texas at Austin, Austin, Texas 78712-1186, United States

[‡]Department of Chemical Engineering, Stanford University, Stanford, California 94305-5025, United States

[§]Department of Energy Resources Engineering, Stanford University, Stanford, California 94305-4007, United States

ABSTRACT: The understanding of the interaction of water with mineral surfaces is fundamental for the description of solid−liquid interface reactions such as adsorption and desorption of solutes in natural and industrial systems. First-principles calculations can aid in the understanding of these interactions at the molecular level, allowing to formulate mechanistic laws of reaction. In this work, the adsorption of water (H_2O) on forsteritic olivine (Mg_2SiO_4) is studied on the stoichiometric (100) surface using density functional theory (DFT) based electronic structure calculations to predict stability and reactivity of this surface under atmospheric and hydrothermal conditions. The structure and the energetics were analyzed for H_2O interacting at different reactive surface sites comprising magnesium, silicon, and oxygen atoms showing that H_2O can be adsorbed molecularly, dissociatively, or in some combination of the two. *Ab initio* thermodynamics was employed to extend the first-principles DFT calculations at 0 K in vacuum to atmospheric and hydrothermal conditions providing predictions of the changes in surface stability as a function of temperature and pressure. The type of interaction was analyzed through the surface energy, Bader charge analysis, and the projected density of state (PDOS) of the most stable hydroxylated surface over a wide range of temperatures. This analysis shows that the most stable configuration is the adsorption of two water molecules on two surface sites leading to the formation of a hydronium ion, H_3O^+, bridging two Mg1 atoms and elongating their bonds with the surrounding surface oxygen atoms and a H^+ binding to a Si atom. Bader charge and density of states analyses indicate that upon interaction significant charge is lost from the surface atoms toward the water molecule groups, suggesting that the hydronium ion is chemisorbed at the Mg surface atoms resulting in reduced stability compared to the Si atom. Finally, the coverage effect up to two layers of water molecules (20 H_2O/nm^2) was investigated to validate our calculations. Below 6 H_2O/nm^2, our calculations agree with previous DFT studies available at low coverage predicting that water dissociates at the most reactive sites. At higher coverage, our energetics agree with the experimental data from calorimetric measurements and show that at the most stable hydrated surface water can both dissociate and be molecularly adsorbed, thereby creating a hydrogen-bonding network involving the first and the second water layer.

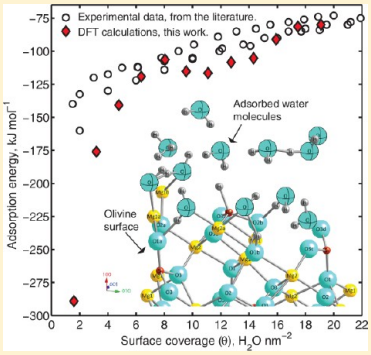

INTRODUCTION

Olivine ($(Mg,Fe)_2SiO_4$) is a solid solution of forsterite (the magnesium end member, Mg_2SiO_4) and fayalite (the iron end member, Fe_2SiO_4). It is the most abundant silicate in the Earth's upper mantle, and because of its prominent occurrence and its high reactivity with water (H_2O) and carbon dioxide (CO_2), it has been widely investigated at various thermodynamic conditions. There has been recent interest with respect to the interaction of olivine for its potential use in carbon capture, utilization, and storage (CCUS) technologies to permanently fix CO_2 into stable carbonate minerals under hydrothermal conditions.[1]

In the presence of H_2O and CO_2, olivine undergoes hydration (or serpentinization) followed by dissolution and carbonation. To describe these processes, it is crucial to understand the interaction of water with olivine in aqueous and humid systems. Despite the numerous theoretical and experimental studies over a range of scales, the mechanism of interaction between water and olivine is still uncertain. The most extensive experimental studies have been carried out to study the interaction of water with olivine at the microscale with the aim to characterize its dissolution kinetics.[2−11] Among these studies, the results reported in Awad et al.[4] on the directional dissolution along the crystallographic axes allow for the interpretation of the mechanism at the microscale on the basis of the phenomena occurring at the molecular scale. The study suggests that the dissolution kinetics is affected by the electronic structure of the mineral surfaces as the dissolution rates change along specific axes. Under atmospheric and hydrothermal conditions (up to 140 °C), relevant for CCUS, the slowest dissolution is obtained along the *a*-axis, i.e., for the (100) surface.

Theoretical studies based on DFT performed by de Leeuw,[12] Stimpfl et al.,[13] and King et al.[14] have focused on the hydration of the magnesium end member of olivine, i.e., forsterite, and have shown that forsterite upon hydration becomes more

Received: April 2, 2013
Revised: August 19, 2013
Published: August 20, 2013

   dx.doi.org/10.1021/jp403271e | *J. Phys. Chem. C* 2013, 117, 21203−21216

thermodynamically stable and that the interaction involves specific sites, of which some lead to the dissociation of water (dissociative adsorption) and others to the adsorption of undissociated water (molecular adsorption). The preference of one mechanism over the other depends on the electronic structure of the surface as well as on its thermodynamic stability. On the most thermodynamically stable (010) surface,[15,12] water is adsorbed molecularly, while it is dissociatively adsorbed on the second most stable (100) surface.[14] The surface affinity to water depends on the coordination of the surface sites, with the strongest interaction observed at the uncoordinated Mg ions.[13,14] Despite this previous investigation of the water−forsterite interaction, these studies are, however, limited by the extension of the investigated surface coverage, with less than a monolayer of water considered, i.e., approximately 2 H_2O/nm^2. Furthermore, the calculations have been restricted to 0 K in vacuum and have not been verified against laboratory measurements.

Recent experimental studies have focused on forsterite hydration investigating the interaction of water with forsterite at the nanoscale. Calorimetric measurements performed by Chen and Navrotsky[16] and spectroscopy measurements by Loring et al.[17] have shown that at both atmospheric and hydrothermal conditions approximately two layers of ordered water molecules, corresponding to 10 H_2O/nm^2 per layer, form on the forsterite surface. The water molecules interact significantly with the mineral surface and are therefore responsible for changing the atomic and electronic structure of the surface. Molecular dynamic simulations performed by Kerisit et al.[18] for the forsterite (010) surface agree partially with these measurements, only at high coverage of approximately 20 H_2O/nm^2, suggesting that three monolayers of ordered water molecules form instead of two. From the first layer, the closest to the interface, to the third layer, the coverage changes as 7.0, 6.8, and 8.8 H_2O/nm^2, respectively. Above the third layer, water exhibits bulk behavior and weakly interacts with the mineral surface. Similar studies on mineral hydration have been carried out by Catalano et al.[19,20] to characterize the interaction of water with corundum (α-Al_2O_3) (012) and with hematite (Fe_2O_3) surfaces. Their measurements based upon high-resolution specular X-ray reflectivity show that two layers of adsorbed water molecules form on the mineral surface termination with a faster decay of the ordering on corundum than on hematite, possibly as a consequence of a more significant reduction of the electron density at the interface of Fe_2O_3 than of α-Al_2O_3. Similar hypotheses were later verified by Aboud et al.[21] and Lo et al.[22] through DFT calculations.

These theoretical and experimental investigations suggest that the formation of the ordered water layers is typical of a solid surface and depends on the electronic structure of the mineral interface and, furthermore, in order to characterize the interactions of water with mineral surfaces, even in a bulk aqueous system, the analysis can be restricted to a system comprising the ordered water layers in the proximity of the water−mineral interface.

In this work, DFT calculations have been carried out to investigate the mechanism of the hydration of forsterite onto the stoichiometric (100) surface. The energetics were determined at 0 K in a vacuum and then extrapolated to atmospheric and hydrothermal conditions using *ab initio* thermodynamics. The stability and the reactivity of the surface were investigated by combining the energy of adsorption with the surface energy at various temperatures and pressures in conjunction with a Bader charge analysis and projected density of state analysis (PDOS). Finally, the calculations were verified based upon earlier theoretical calculations and experimental data of calorimetric measurements through the analysis of the coverage effect.

OLIVINE CRYSTAL STRUCTURE

Olivine crystallizes in the orthorhombic system (space group *Pbnm*), and in a given unit cell, there are four formula units containing 28 atoms, i.e., 8 iron/magnesium (Fe/Mg), 4 silicon (Si), and 16 oxygen (O) atoms. The key structural unit is a serrated chain of cation-octahedra (Mg and Fe) lying parallel to the *c*-axis and joined together by the silicon-centered tetrahedra.[4,23] In the olivine structure, the oxygen atoms occupy three different positions, i.e., O1, O2, and O3, in both the Mg-octahedra and the Si-tetrahedra. Each Si atom is tetrahedrally coordinated with four oxygen atoms with two of them being O3 and equidistant from the silicon atom, while O1 is the farthest and O2 is the closest. The Mg and Fe atoms are coordinated with six oxygen atoms and occupy two different sites in the structure, namely, M1 and M2. The M1 oxygen atom is held in a distorted octahedron with two O1, two O2, and two O3 atoms held at the apexes connected by two Si-tetrahedral edges, while M2 is in a less-distorted octahedron surrounded by one O1, one O2, and four O3 atoms connected to one tetrahedral edge and three tetrahedral apexes.[24]

In this work, we focus on the study of the interaction of H_2O with the Mg end member of olivine, i.e., forsterite (Mg_2SiO_4), containing Mg atoms in both M1 and M2 sites. The forsterite crystal structure is shown in Figure 1 with the M1 and M2 sites indicated as Mg1 and Mg2, respectively.

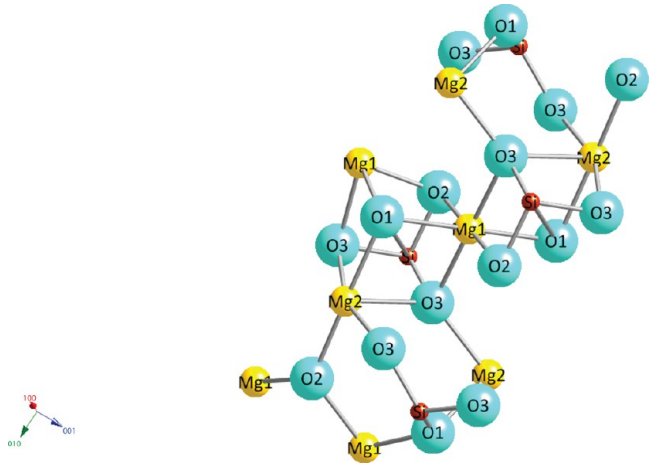

Figure 1. Forsterite (Mg_2SiO_4) unit cell. Magnesium atoms are indicated in yellow, silicon atoms in red, and oxygen atoms in cyan. The directions correspond to (100) *a*-axis, (010) *b*-axis, and (001) *c*-axis.

METHODS

Computational Methodology. Periodic *ab initio* DFT calculations were performed using the Vienna *ab initio* Simulation Package (VASP),[25] which is a computational tool used to calculate the electronic properties of atoms and molecules in a given system. In this work, simulations were performed using the Perdew−Burke−Enzerhoff (PBE)[26] generalized gradient approximation (GGA) with the motion effects of the core electrons and their nuclei replaced by an effective core potential or pseudopotential. The pseudopotential employed in this work was based upon the projector-augmented waves (PAW) type[27,28] with an optimized cutoff energy of 460 eV.

dx.doi.org/10.1021/jp403271e | J. Phys. Chem. C 2013, 117, 21203−21216

The density of *k*-points was determined on the basis of the convergence criterion of 10^{-4} eV for the total energy of the bulk and the minimization of the computational time using the experimental value of the lattice constant as a starting guess. A $4 \times 2 \times 4$ *k*-point mesh for the Brillouin zone (BZ) was chosen according to a Monkhorst–Pack[29] of $4 \times 2 \times 4$. The optimized lattice parameters *a*, *b*, and *c* of the Mg_2SiO_4 bulk unit cell are reported in Table 1 and are in agreement with the experimental

Table 1. Comparison of Calculated and Experimental Structural Parameters of Forsterite

	a (Å)	*b* (Å)	*c* (Å)	α (deg)	β (deg)	γ (deg)
this work	4.809	10.364	6.063	90	90	90
experimental						
ref 30	4.756	10.207	5.980	90	90	90
ref 31	4.753	10.190	5.978	90	90	90
previous DFT calculations						
ref 32	4.710	10.150	5.960	90	90	90
ref 12	4.781	10.297	6.011	90	90	90

measurements and previous DFT calculations. The total energy of one unit cell with the applied level of theory of the bulk is as large as −48.207 eV.

The Mg_2SiO_4 (100) surface was simulated using a $4 \times 1 \times 1$ unit cell ($19.235 \times 10.364 \times 6.0627$ Å^3), which corresponds to a four-layer slab with symmetry. This four-layer thickness ensured bulk-like behavior of the first three unit cells along the principal direction without imposed constraints. The number of *k*-points used was $1 \times 2 \times 4$ and was determined through a convergence analysis of the total energy of the surface with 0.01 eV accuracy.

During the calculations, the bottom layer was maintained fixed and the dipole correction was included. The Mg_2SiO_4 (100) surface was composed of stoichiometric layers, and thus it had no dipole perpendicular to the surface.[15] However, in our simulations the water molecules are allowed to interact with the surface only on one side of the slab, breaking its symmetry; therefore, a dipole correction was employed. In addition, to cancel any dipole moment that could have been created due to the periodical boundary conditions, the periodic images of the unhydrated surfaces of the slabs were separated by a vacuum space of 20 Å along the *a*-axis, which allows for at least 15 Å of distance between the periodic images of the hydrated surfaces guaranteeing minimal interaction between neighboring layers.

The structure of gas-phase water (H_2O_{gas}) was calculated as an isolated molecule in a $25 \times 25 \times 25$ Å^3 periodic box. The optimized structure has a bond length of 0.972 Å and an angle of 104.65°, which are in agreement with the experimental values of 0.958 Å and 104.51°,[33] respectively. The minimum Gibbs free energy associated with this geometry is −14.217 eV, which is slightly larger than −14.140 eV calculated by de Leeuw.[12] However, it is well-known that DFT total energy calculations for gaseous molecules, such as water, are less accurate than for extended systems such as bulk or surfaces; therefore, the comparison can be considered satisfactory.

Adsorption Energy. To determine the stability of the Mg_2SiO_4 (100) surface upon interaction with gaseous water, the adsorption energy (or binding energy) (E_{ads}, eV) was calculated as

$$E_{ads} = \frac{1}{n}(E_{hydr} - E_{clean} - nE_{H_2O_{gas}}) \quad (1)$$

where E_{hydr} is the total energy of the hydrated Mg_2SiO_4 (100) surface, eV; E_{clean} is the total energy of the dehydrated Mg_2SiO_4 (100) surface, eV; $E_{H_2O_{gas}}$ is the total energy of the gaseous water molecule, eV; and *n* is the total number of water molecules interacting with the surface. A large negative value of E_{ads} indicates a strong interaction between the surface and the water molecule, and the minimum value corresponds to the most thermodynamically stable configuration. To ensure the determination of the global minimum for each given water–surface configuration, different starting geometries were tested and the minimum was then considered.

***Ab Initio* Thermodynamics.** *Ab initio* thermodynamics was employed to extrapolate the energetics determined at 0 K in vacuum to the thermodynamic conditions relevant for our application. At this aim, the surface free energy (γ, eV/Å^2) was determined over a range of temperature (T) and pressure (P) values. The surface free energy of a semi-infinite slab with one reactive surface in contact with a gas-phase reservoir at a given T and P is given by

$$\gamma(T, P, \{N_i\}) = \frac{1}{A}(G(T, P, \{N_i\}) - \sum_{i=1}^{n} N_i\mu_i(T, P)) \quad (2)$$

where $G(T,P,\{N_i\})$ is the Gibbs free energy of the system consisting of the forsterite surface and the adsorbed water molecules, eV; N_i is the number of moles of the *i*th atom in the system, i.e., Mg, O, Si, and H; μ_i is the chemical potential of the *i*th atom, eV; and *A* is the cross-sectional area of the surface, Å^2. For the Mg_2SiO_4 surface reacting with water, eq 2 becomes

$$\gamma(T, P, \{N_i\}) = \frac{1}{A}(G_{surf} - N_{Mg}\mu_{Mg} - N_O\mu_O - N_{Si}\mu_{Si} - N_H\mu_H) \quad (3)$$

Considering the Gibbs free energy of the surface water system as[34]

$$G_{surf} = E^{total} + F^{vib} + F^{conf} + PV \quad (4)$$

where E^{total} is the total energy determined through DFT calculations at constant volume, eV; F^{vib} is the vibrational free energy, eV; F^{conf} is the configurational free energy, eV, negligible below 1000 K; and the last term corresponds to the free energy contribution from the pressure and the volume of the system, eV, which becomes negligible below 100 atm. Therefore, eq 4 can be simplified to

$$G_{surf} = E^{total} + F^{vib} \quad (5)$$

Generally, in a water–mineral surface system the important contribution to F^{vib} is from the vibrational energy of the hydrogen atoms of the adsorbed gaseous water molecule;[35] therefore

$$F^{vib} = \sum_{k=1}^{N}\left[\frac{\hbar\omega_k}{2} + k_BT\ln(1 - e^{-\hbar\omega_k/k_BT})\right] \quad (6)$$

where *N* is the total number of the vibrational modes of the adsorbed hydrogen atoms; ω_k is the vibrational frequencies, (s^{-1}); T is the temperature, K; $\hbar$ is the reduced Planck's constant, and k_B is the Boltzmann constant. The vibrational frequencies ω_k were calculated by starting with the equilibrated hydrated structures, fixing all the atomic coordinates except those of the hydrogen atoms in the water molecules, and then extracted by diagonalizing the mass-weighted Hessian matrix.

dx.doi.org/10.1021/jp403271e | J. Phys. Chem. C 2013, 117, 21203–21216

The chemical potential of the solid phase is a linear combination of the chemical potential of each individual atom comprised in the phase, i.e., Mg, O, and Si, and is given by

$$\mu_{Mg_2SiO_4}(T, P) = 2\mu_{Mg}(T, P) + 4\mu_{O}(T, P) + \mu_{Si}(T, P) \quad (7)$$

which at equilibrium equals $G_{Mg_2SiO_4}(T,P)$. Similarly, the chemical potential of the water molecules in the system is

$$\mu_{H_2O}(T, P) = 2\mu_{H}(T, P) + \mu_{O}(T, P) \quad (8)$$

which can be determined considering the following thermodynamic relationship:

$$\mu_{H_2O}(T, P) = E^{total}_{H_2O} + E^{ZPE}_{H_2O} + \mu_{H_2O}(T, P_0) + k_B T \ln\left(\frac{P}{P_0}\right) \quad (9)$$

where $E^{total}_{H_2O}$ is the total energy of the isolated water molecule estimated from DFT calculations and as large as −14.217 eV; $E^{ZPE}_{H_2O}$ is the zero-total vibrational energy at 0 K in vacuum, also determined through DFT calculations and equal to 0.568 eV; $\mu_{H_2O}(T,P_0)$ is the "temperature dependent chemical potential", which includes the contributions from vibrations and rotations at the standard pressure P_0 of 1 atm, eV; and the last term in the equation represents the chemical potential associated with the variation of the temperature and pressure of the system. The values of $\mu_{H_2O}(T,P_0)$ were determined using the NIST-JANAF thermodynamic tables[36] assuming humid thermodynamic conditions and considering the following thermodynamic relationship:[35]

$$\mu_{H_2O}(T, P_0) = H(T, P_0) - H(0, P_0) - T(S(T, P_0) - S(0, P_0)) \quad (10)$$

where H is the enthalpy, kJ/kg, and S is the entropy, kJ/(kg K).

Substituting eqs 7 and 8 in eq 3, the surface free energy becomes

$$\gamma(T, P, \{N_i\}) = \frac{1}{A}(G_{surf} - N_{Si}G_{Mg_2SiO_4} - N_O\mu_{H_2O}) \quad (11)$$

where $G_{Mg_2SiO_4}$ is the Gibbs free energy of one unit cell of forsterite determined upon bulk optimization.

RESULTS AND DISCUSSION

Optimized Structure of the Stoichiometric Mg_2SiO_4 (100) Surface. The analysis of the interaction of water with forsterite was performed by considering the adsorption of gaseous water molecules on the stoichiometric Mg_2SiO_4 (100) surface. Various geometries of the H_2O−Mg_2SiO_4 (100) system were investigated using a four-layer slab without steps or imperfections as shown in Figure 2a. To verify the accuracy of our calculations, the bond distance in the inner layers was calculated upon relaxation and compared with the corresponding bond distance in the bulk. By fixing the first layer, the bond distances in the two central layers changed less than 1%, indicating that the layers exhibit bulk-like behavior, while the upper layer had a more pronounced deformation, as expected.

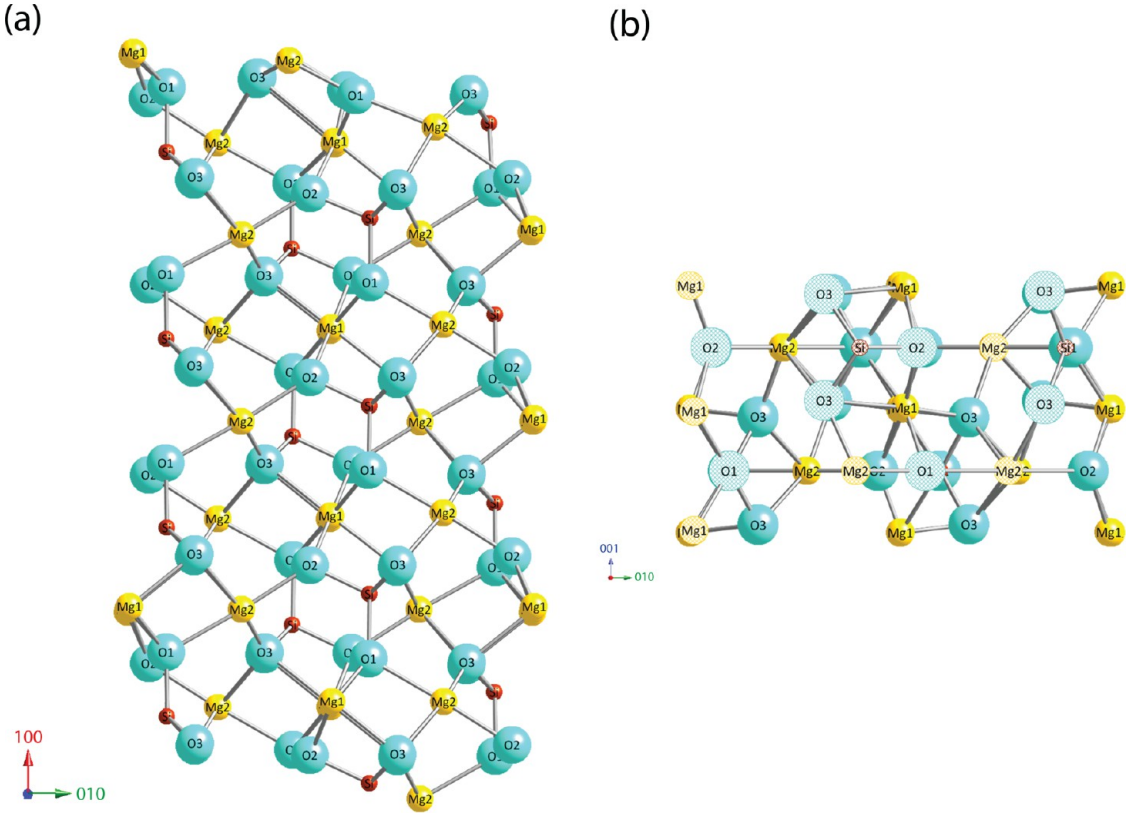

Figure 2. Clean Mg_2SiO_4 (100) surface where magnesium atoms are indicated in yellow, silicon atoms in red, and oxygen atoms in cyan. (a) View of the four-layer Mg_2SiO_4 slab along the (001) direction corresponding to the *c*-axis. (b) Top view of the Mg_2SiO_4 (100) surface along the direction (100) corresponding to the *a*-axis. The hatched style in (b) highlights the 14 atoms on the topmost layer of the slab considered in the interaction with water.

dx.doi.org/10.1021/jp403271e | J. Phys. Chem. C 2013, 117, 21203−21216

Upon relaxation, the topmost area of the (100) surface is as large as 10.364 × 6.063 Å^2, and the surface energy per formula unit of the slab at 0 K is 0.259 eV/Å^2, which corresponds to 4.16 J/m^2 and is in agreement with the experimental value of 4.41 ± 0.21 J/m^2 reported by Chen and Navrotsky.[16]

The interaction with water was performed by placing the molecules on the topmost part of the slab, which is shown in Figure 2b.

Adsorption Energy and Geometry. The adsorption of water was analyzed on the (1 × 1)-unreconstructed Mg_2SiO_4 (100) surface. The stoichiometric (100) Mg_2SiO_4 termination presents 14 ionic adsorption sites, i.e., not fully coordinated atoms. We performed preliminary calculations to investigate their reactivity with water. From a total number of 14 reactive sites identified initially, only 12 manifested significant reactivity bonding the water molecule through either associative (molecular) or dissociative adsorption. The negligible interaction observed at the two sites, comprising Mg2 and Si atoms, is due to their location deep in the surface structure where the steric effect of the surrounding surface oxygen atoms is strongly pronounced.[13] A top view of the (100) surface with indicated the 12 surface sites is shown in Figure 3.

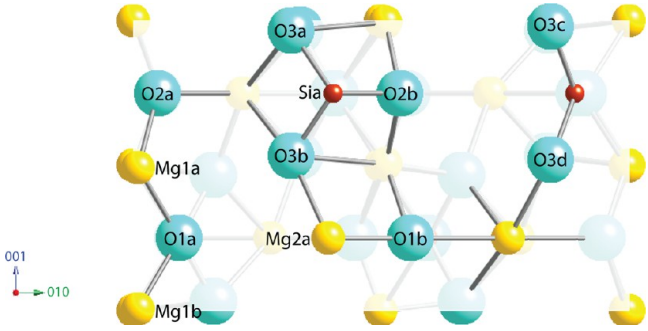

Figure 3. Top view of the Mg_2SiO_4 (100) surface with the 12 tested surface sites as labeled accordingly.

To allow interaction between either the oxygen or the hydrogen in the water molecule and the surface site atom, an initial distance of 1.1−1.9 Å was chosen. To avoid symmetry effects, the water molecule was displaced 0.2 Å apart from the site in any symmetric direction on the surface plane (100). Several different initial water−surface configurations were tested, and the most stable one, i.e., the one resulting with the lowest adsorption energy calculated through eq 1, was then selected.

The values of the adsorption energy (E_{ads}, eV per water molecule) and surface energy (γ, eV/Å^2) are listed in Table 2 for two values of coverage (θ, defined as the ratio between the number of adsorbed H_2O molecules and the surface area, H_2O/nm^2) equal to 1.59 and 3.18 H_2O/nm^2. In the case of low coverage, the water molecule was placed with the H−O−H axis either along the (100) direction or orthogonal to the (100) direction, thereby bridging two oxygen surface atoms. While in the case of large coverage, two water molecules were placed close to distinct sites with their H−O−H axis along the (100) direction.

At coverage 1.59 H_2O/nm^2, the most stable hydrated surfaces are those where the water molecule dissociates. Water predominantly results in an OH group interacting with the surface oxygen atom and a H atom interacting with a metal surface site. Configurations where dissociative adsorption arises show a significant surface reconstruction in comparison to configurations where molecular adsorption occurs. This may be responsible for the low adsorption energies calculated which are in some cases less than −3 eV per H_2O molecule. Only two sites containing oxygen atoms do not interact in a dissociative way, namely O1b and O3d. However, their corresponding adsorption energies are still significant, approximately between −1 and −2 eV per H_2O molecule. Among the remaining three Mg atoms, the Mg1b site is the most reactive site, while the Mg2a site has the weakest interaction. Examples of initial and final geometries where water is adsorbed molecularly at the Mg1b surface site and dissociatively at the O2a site are shown in Figures 4 and 5, respectively. Here, part a shows the initial geometry and parts b−d show the final geometry from different directions.

Our results agree with earlier DFT calculations reported by King et al.[14] for the hydrated Mg_2SiO_4 (100) termination as we predict an average E_{ads} as large as −1.304 and −2.995 eV per H_2O molecule for molecular and dissociative adsorption, respectively, while King et al. report −1.658 and −3.319 eV per H_2O molecule, respectively. Overall, our analysis suggests that when the water molecule is adsorbed nearby O2 and O3 surface atoms, an OH group forms at the O2 and O3 atoms and the resulting hydrated Mg_2SiO_4 (100) surfaces are the most stable. This observation agrees partially with those ones made by Kudoh et al.[37] and by Liu et al.[38] which indicate that the O2 and O3 atoms are the most probable adsorption sites but only for protons. Nevertheless, the study by Kudoh was restricted to just the adsorption of protons while the one by Liu et al. was based on molecular simulations for the hydrated Mg_2SiO_4 (001) surface.

Surface reconstruction was analyzed through the determination of the surface deformation, i.e., the changes in the angle, bond, and interlayer distances upon water adsorption with respect to the clean surface. The values of deformation are reported in parentheses in Figures 4 and 5. In the case of molecular adsorption the surface reconstruction is clearly negligible given the small variations in the bond lengths and the interlayer distances with respect to the stoichiometric surface. This negligible surface reconstruction indicates a weak interaction between the water and the surface site. The opposite effect is seen in the case of dissociative adsorption, clearly evident in Figure 5b. Initially, the water molecule was placed close to the O2a surface site, and upon interaction the water dissociates producing an OH group bridging Mg1a and Mg1b surface sites with a hydrogen atom bound to Sia. The pronounced reconstruction of the surface upon dissociative adsorption indicates a strong interaction between water and the subsequent formation of a covalent bond.[22]

At coverage 3.18 H_2O/nm^2, two water molecules simultaneously interact with two surface sites; one molecule is placed nearby the O2a surface site while the other nearby one of the remaining free. The O2a site was selected because its interaction with water led to the most stable hydrated surface at the lowest coverage. In the tested configurations, water is adsorbed both in a molecular and in a combination of molecular and dissociative ways (mix adsorption). However, mixed adsorption is predominant and manifests itself with one water molecule dissociating at the O2a site in the same way observed at coverage 1.59 H_2O/nm^2, and with a second water molecule either adsorbed molecularly or bounded to the OH group produced by the dissociated H_2O molecule. Configurations in which mixed adsorption arises show a significant surface reconstruction in comparison to configurations where only molecular adsorption occurs. This may explain the low adsorption energies calculated,

dx.doi.org/10.1021/jp403271e | J. Phys. Chem. C 2013, 117, 21203−21216

Table 2. Adsorption Energy (E_{ads}, eV) and Surface Energy (γ, eV/Å^2) Calculated at 0 K in Vacuum Using Eqs 1 and 2 with Corresponding Adsorption Mechanism[a]

surface site	E_{ads} (eV/H_2O)	γ (eV/Å^2)	adsorption mechanism
		θ = 1.59 H_2O/nm^2	
Mg2a	−0.791	0.247	Mol
Sia	−0.976	0.244	Mol
O2b-H_2O-O1b	−1.071	0.216	Mol
Mg1a	−1.075	0.244	Mol
O3d	−1.139	0.245	Mol
O3a	−1.755	0.233	Mol
Mg1b	−2.089	0.227	Mol
O1b	−1.582	0.236	Dis; O1b-H, Mg2a-OH
O1a	−2.100	0.232	Dis; O1a-H, Mg1a-OH-Mg1b
O2b	−2.682	0.219	Dis; O2b-H, Sia−OH
O1a-H_2O-O3b	−3.010	0.215	Dis; O3b-H, O1a-HO
O1b-H_2O-O3d	−3.021	0.216	Dis; O3d-H, Mg1a-OH
O2a-H_2O-O3b	−3.041	0.213	Dis; O3a-H, Mg1b-OH
O3a-H_2O-O3b	−3.194	0.211	Dis; O3b-H, Mg1a-OH
O3b	−3.311	0.203	Dis; O3b-H, Mg1a-OH-Mg1b
O1a-H_2O-O2a	−3.531	0.206	Dis; O3b-H, Mg1a-OH
O2a-H_2O-O3a	−3.536	0.205	Dis; O3a-H, Mg1b-OH
O3c	−3.596	0.206	Dis; O3c-H, Mg1a-OH-Mg1b
O2a	−4.700	0.185	Dis; Sia-H, Mg1a-OH-Mg1b
		θ = 3.18 H_2O/nm^2	
H_2O-O2a,H_2O-O3d	−1.161	0.222	Mol
H_2O-O2a,H_2O-Sia	−1.254	0.223	Mol
H_2O-O2a,H_2O-O3b	−1.282	0.220	Mol
H_2O-O2a,H_2O-O1b	−1.445	0.220	Mix; Sia-H, Mg1a-OH-Mg1b, HOH-O1b
H_2O-O2a,H_2O-Mg2a	−1.666	0.204	Mix; Sia-H, Mg1a-OH-Mg1b, HOH-Mg2a
H_2O-O2a,H_2O-O1a	−2.321	0.189	Mix; Sia-H, Mg1a-OH-Mg1b, HOH-O1a
H_2O-O2a,H_2O-O3c	−2.432	0.190	Mix; Sia-H, Mg1a-OH-Mg1b, HOH-O3c
H_2O-O2a,H_2O-Mg1a	−3.034	0.156	Mix; Sia-H, HOH-Mg1a-OH-Mg1b

[a]The surface sites are identified as in Figure 3.

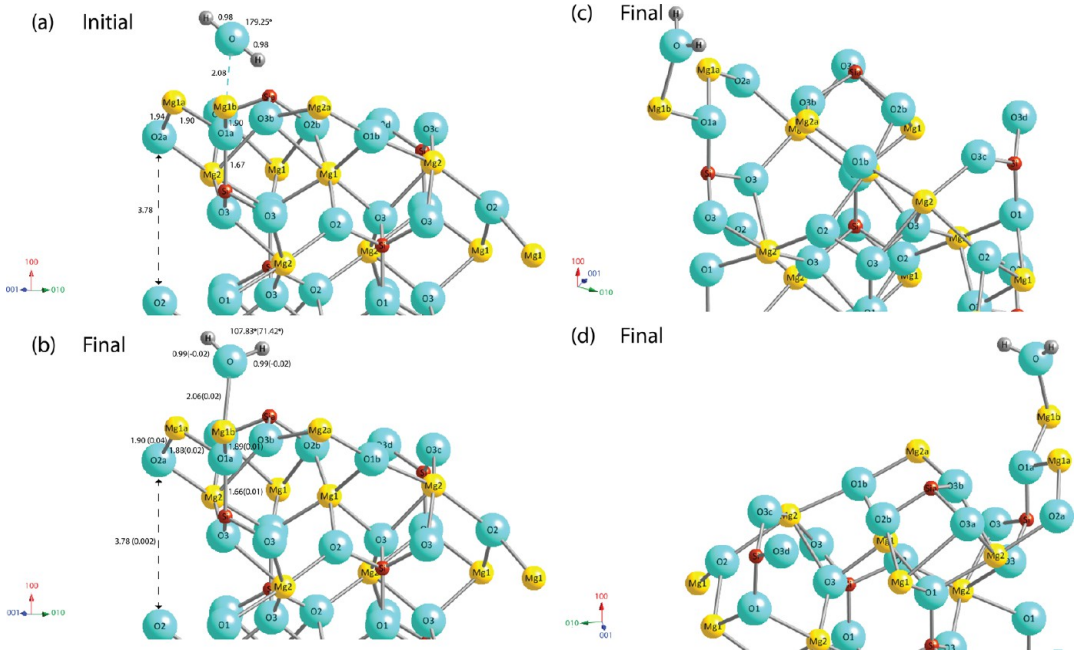

Figure 4. Initial (a) and final (b−d) surface geometries of the most stable water−forsterite configuration for molecular adsorption. Angle, bond, and interlayer distances are given with the changes calculated with respect to the initial surface in parentheses.

which are in some cases smaller than −3 eV per H_2O molecule. Only three sites containing oxygen do not interact in a dissociative way, namely O3d, Sia, and O3b. However, their corresponding adsorption energies are still significant, approximately −1.2 eV per H_2O molecule. The lowest adsorption energy is attained where one water molecule is placed nearby the

dx.doi.org/10.1021/jp403271e | J. Phys. Chem. C 2013, 117, 21203−21216

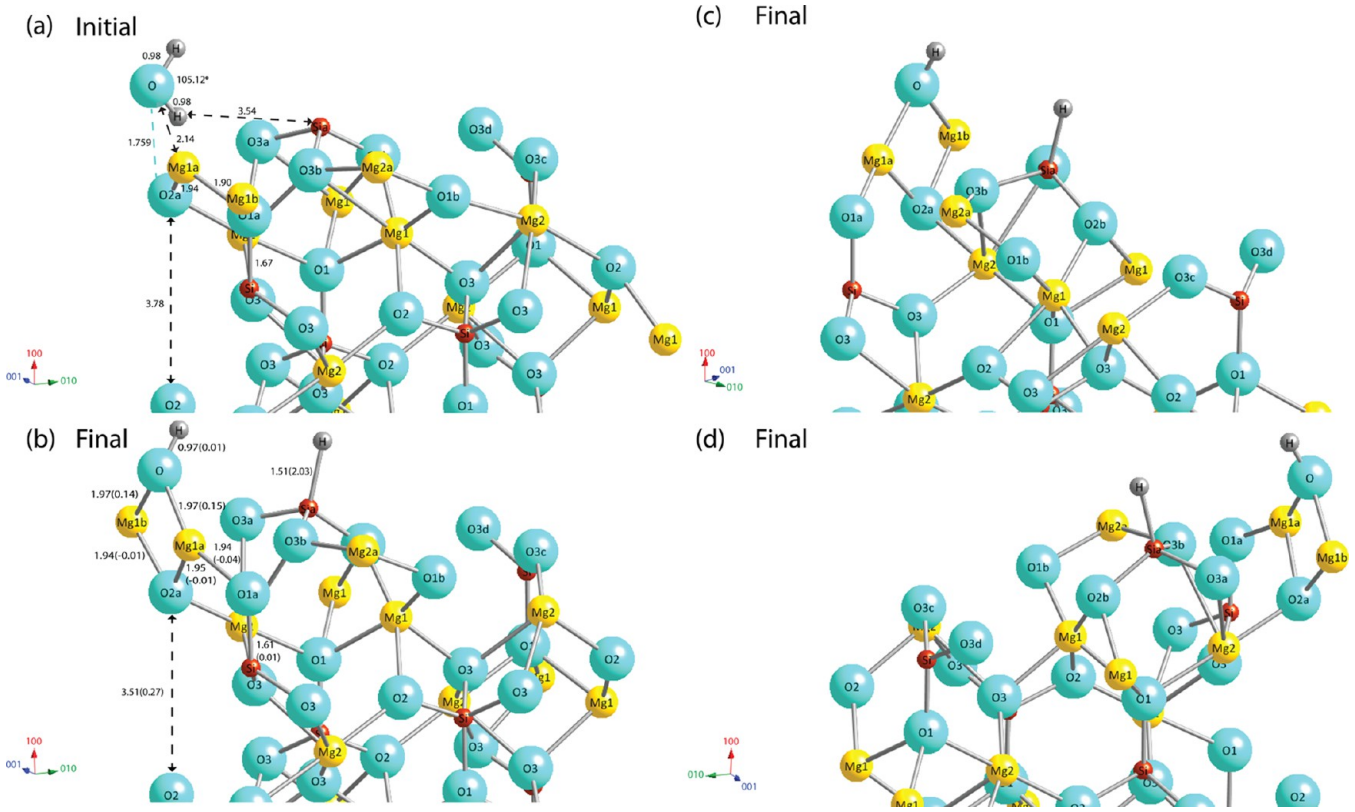

Figure 5. Initial (a) and final (b–d) surface geometries of the most stable water–forsterite configuration for dissociative adsorption. Angle, bond, and interlayer distances are given with the changes calculated with respect to the initial surface in parentheses.

O2a site and one nearby the Mg1a site. The initial and final geometries for this case are illustrated in Figure 6. Upon interaction, one water molecule dissociates producing an OH group bridging Mg1a and Mg1b surface sites and a hydrogen atom bound to the Sia surface site, similarly to the results where only one water molecule interacts with the O2a site. The second water molecule nearby the Mg1a site does not dissociate, but rather reacts with the OH group of the first water molecule thereby forming a hydronium ion, which bridges the Mg1a and Mg1b surface sites. The pronounced reconstruction of the surface indicated by the elongation of the Mg–O bonds in Figure 6 suggests a strong interaction between the water molecule and the surface site.

To confirm these results and understand the type of water–surface interaction, the analyses of the Bader charge and of the density of states (DOS) were performed. The results are present and discussed in the following sections.

***Ab initio* Thermodynamics.** The results of the thermodynamic stability analysis of the hydrated Mg_2SiO_4 (100) surface terminations are reported and discussed in this section. *Ab initio* thermodynamics investigations were employed to extrapolate the surface free energy, γ, from 0 K in vacuum to conditions relevant for the applications of our interest, i.e., weathering and CCUS. Figure 7 shows γ as a function of temperature (in the specific range of 200–500 K) and at two partial pressures of H_2O (P_{H_2O}), namely 0.032 and 1.015 bar, which correspond to saturated water atmosphere at 298.15 and 393.15 K, respectively. The surface free energy was calculated using eq 11 for all hydrated Mg_2SiO_4 (100) surfaces presented in Table 2. In Figure 7, only γ for the most stable terminations of each mode of interaction are shown, i.e., O2aMg1a, O2a, O2a–H_2O–O3a, and Mg1b. The final geometries of these terminations are then illustrated in Figure 8.

In Figure 7, it is possible to see that γ increases linearly with the temperature and overall decreases with pressure. This indicates that the hydrated surface terminations become less stable with increasing temperature, whereas their stability increases with pressure. The most stable configuration at coverage 1.59 H_2O/nm^2 corresponds to the dissociative adsorption of water nearby the O2a surface site as it is associated with the lowest-lying line in both diagrams, while at coverage 3.18 H_2O/nm^2 the mixed adsorption configuration identified as the O2aMg1a, which consists of two water molecules at the O2a and Mg1a surface sites, is the most stable termination.

Overall, our calculations suggest the adsorption of one proton at the silicon surface site and the hydration of the two magnesium sites is the preferred interaction of water with forsterite. This mechanism partially resembles the observations reported by Kwak et al.[39] In their work, the authors use high-resolution magic-angle spinning (MAS) ^{29}Si, ^{13}C spectroscopy to characterize the hydrated forsterite surface at 80 °C. The MAS NMR spectra show the formation of surface groups consisting of silicon and hydrogen atoms and a surface depletion in magnesium. The authors suggest that upon adsorption of water a Si–OH surface group forms. This hypothesis is in partial agreement with our calculations, which indicate that at the most stable hydrated forsterite termination a direct bond between the silicon surface atom and the hydrogen atom of water forms.

This type of mechanism can be also observed at higher coverage as discussed in the next section.

Bader Charge Analysis. The Bader charge analysis uses the atoms in molecules (AIM) approach, which defines atomic regions (i.e., Bader volumes) within molecules by spatially resolving the minimum electron density of the system. The charge of each atom is calculated by integrating the electronic density within its Bader volume.[40] Because of the different

dx.doi.org/10.1021/jp403271e | J. Phys. Chem. C 2013, 117, 21203–21216

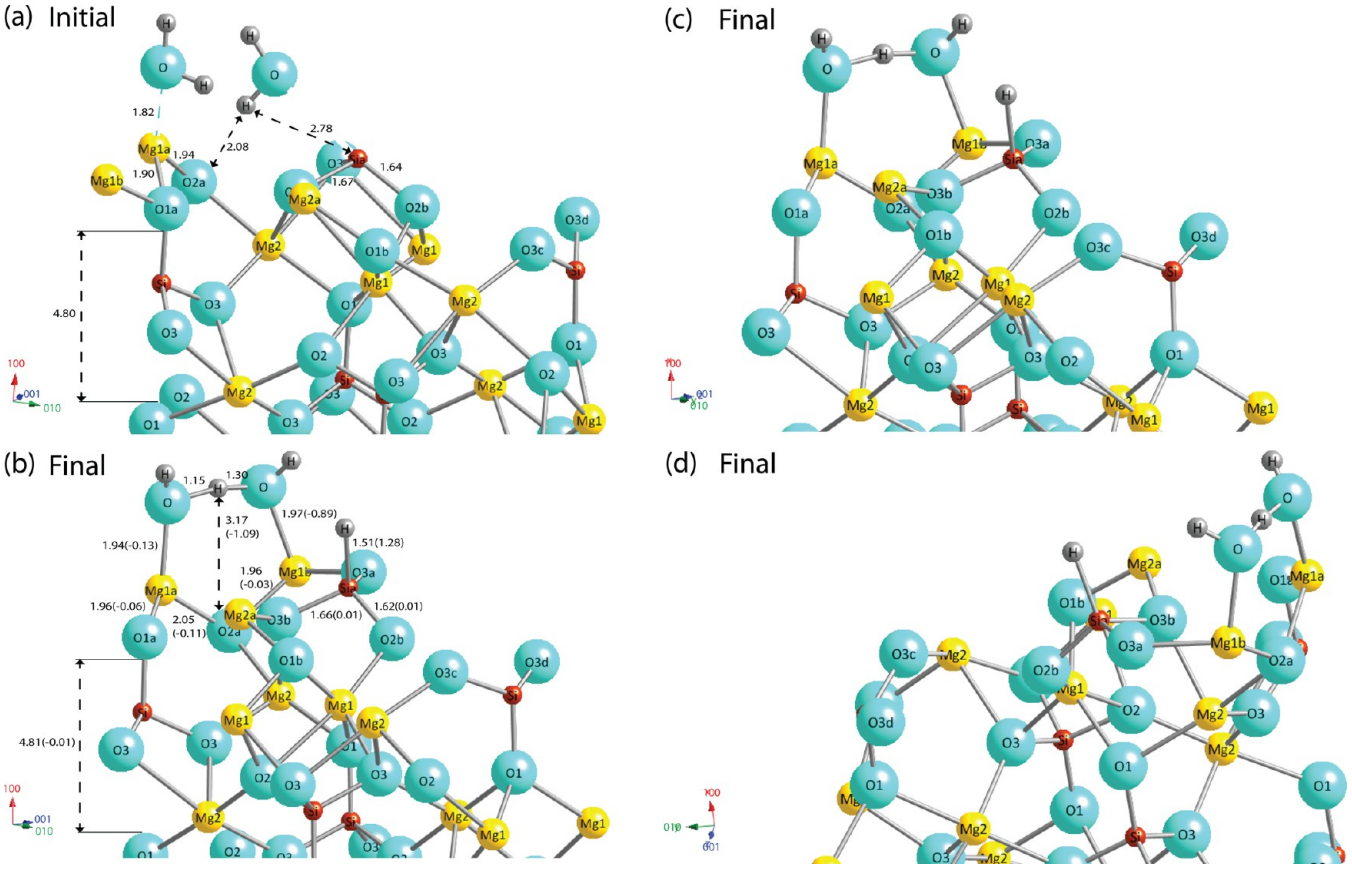

Figure 6. Initial (a) and final (b–d) surface geometries of the most stable water–forsterite configuration for mix adsorption (a combination of molecular and dissociative adsorption). Angle, bond, and interlayer distances are given with the changes calculated with respect to the initial surface in parentheses.

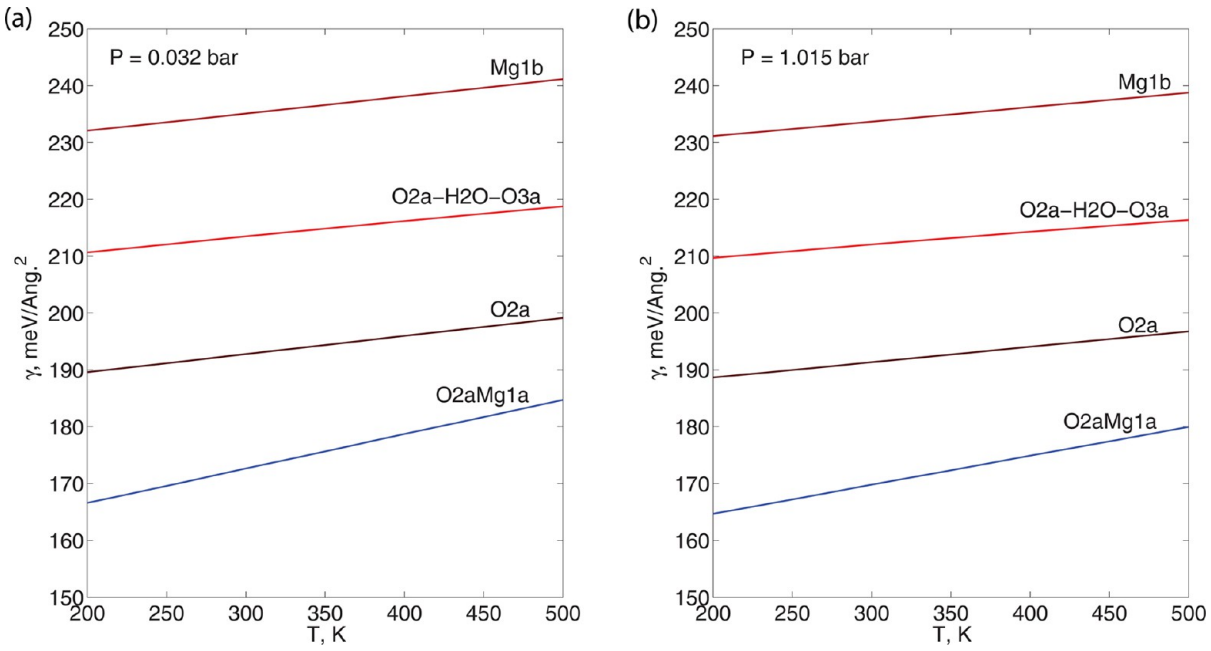

Figure 7. Surface energy as a function of temperature and water saturated partial pressure at 298.15 and 393.15 K. The lines correspond to the four most stable hydrated Mg_2SiO_4 (100) surface terminations in the investigated conditions.

coordination of the atoms in a surface, the same type of atoms may have different charge and thus different chemical reactivity. Therefore, Bader charge analysis may be used as a way to predict the reactivity of a given atom within a surface.

In this work, the reactivity of five of the most stable water–surface configurations has been investigated to determine the charge distribution throughout the adsorption process and is expressed through the charge difference (ΔC, electrons) calculated as

dx.doi.org/10.1021/jp403271e | J. Phys. Chem. C 2013, 117, 21203–21216

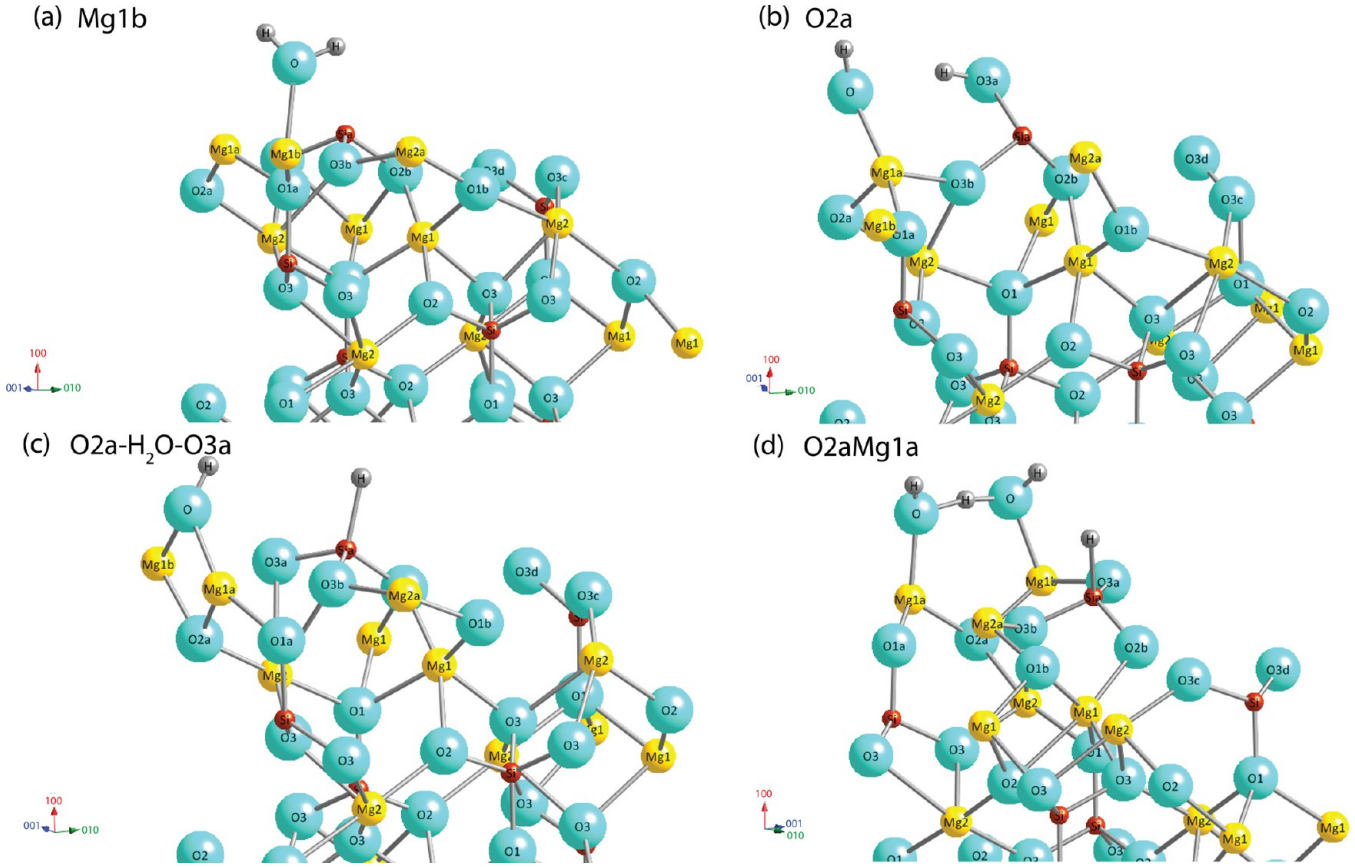

Figure 8. Final surface geometries of the most stable water−forsterite configurations at saturated conditions between 200 and 500 K reported in Figure 7.

$$\Delta C = C_i - C_{\text{hydr}} \tag{12}$$

where C_i, electrons, is either the charge of the isolated clean surface or of the isolated water molecule and C_{hydr}, electrons, is the charge of the surface upon water adsorption. Negative values of ΔC indicate a gain in charge upon adsorption.

In our calculations, the optimized geometry of the hydrated surfaces, the isolated water molecule, and the clean surface were kept fixed, and the source of the isolated water molecule was obtained from the optimized structure of the hydrated systems. The results of the atomic charge differences are summarized in Table 3 as a function of the surface site as labeled in Figure 3. These sites were selected as they have a low adsorption energy and they participate in the formation of hydrated surface groups in the most stable hydrated termination identified as O2aMg1a. The three columns in Table 3 identified by $Mg1a_{str}$, Si_{str}, and $Mg1b_{str}$ list values for surfaces where water is molecularly adsorbed, the $O2a_{str}$ column corresponds to a surface with a single water molecule dissociated, while the last column corresponds to the mixed system where two water molecules have adsorbed both in a molecular and dissociative way.

The greatest charge transfer from the surface to a single adsorbed water molecule system (i.e., 1.478 electrons) corresponds to the water dissociated surface, O2a. This large charge transfer from the surface to the H and OH groups leads to strong binding energy as large as −4.7 eV, as reported in Table 2. Otherwise, small charge changes are observed among the other oxygen surface atoms upon water adsorption. The lowest charge gain corresponds to the Sia_{str} structure (i.e., −0.195 electrons in Table 3), which leads to the lowest adsorption energy in an adsorbed water molecule among all of the surfaces (i.e., −0.976 eV in Table 2). As for the magnesium atoms, Mg1a loses approximately 0.24 electrons to either the H_2O or the OH groups during molecular ($Mg1a_{str}$) and mixed ($O2aMg1a_{str}$) water adsorption. In general, the higher charge changes correspond to

Table 3. Summary of the Atomic Charges (electrons) of the Surface Atoms upon Adsorption of One Water Molecule at the Surface Sites Mg1a, Sia, Mg1b, and O2a and Two Water Molecules at O2a and Mg1a (Sixth Column)[a]

surface site	$Mg1a_{str}$	Sia_{str}	$Mg1b_{str}$	$O2a_{str}$	$O2aMg1a_{str}$
Mg1b	−0.080	−0.141	0.060	0.306	0.204
Mg1a	0.244	−0.142	0.008	0.304	0.241
Mg2a	0.001	−0.015	0.001	−0.001	0.015
O1a	0.007	0.050	0.021	0.027	0.102
O1b	0.001	−0.054	0.006	0.001	0.001
O2b	0.043	0.008	0.008	−0.046	−0.019
O2a	0.038	−0.011	0.020	0.127	0.099
O3c	−0.020	0.007	−0.010	−0.003	0.005
O3d	−0.013	0.007	−0.008	−0.003	0.011
O3a	0.048	0.034	0.022	−0.030	0.048
O3b	0.063	0.034	0.006	−0.020	0.038
Sia	−0.093	0.419	0.053	0.730	0.667
Sib	0.001	0.004	0.000	−0.001	−0.008
ΔC of the surface site	0.240	0.201	0.187	1.394	1.402
ΔC of water molecule	−0.249	−0.195	−0.210	−1.478	−1.473

[a]Here the subscript "str" is included to distinguish the structure as reported in Table 2 from the surface site in the first column.

dx.doi.org/10.1021/jp403271e | J. Phys. Chem. C 2013, 117, 21203−21216

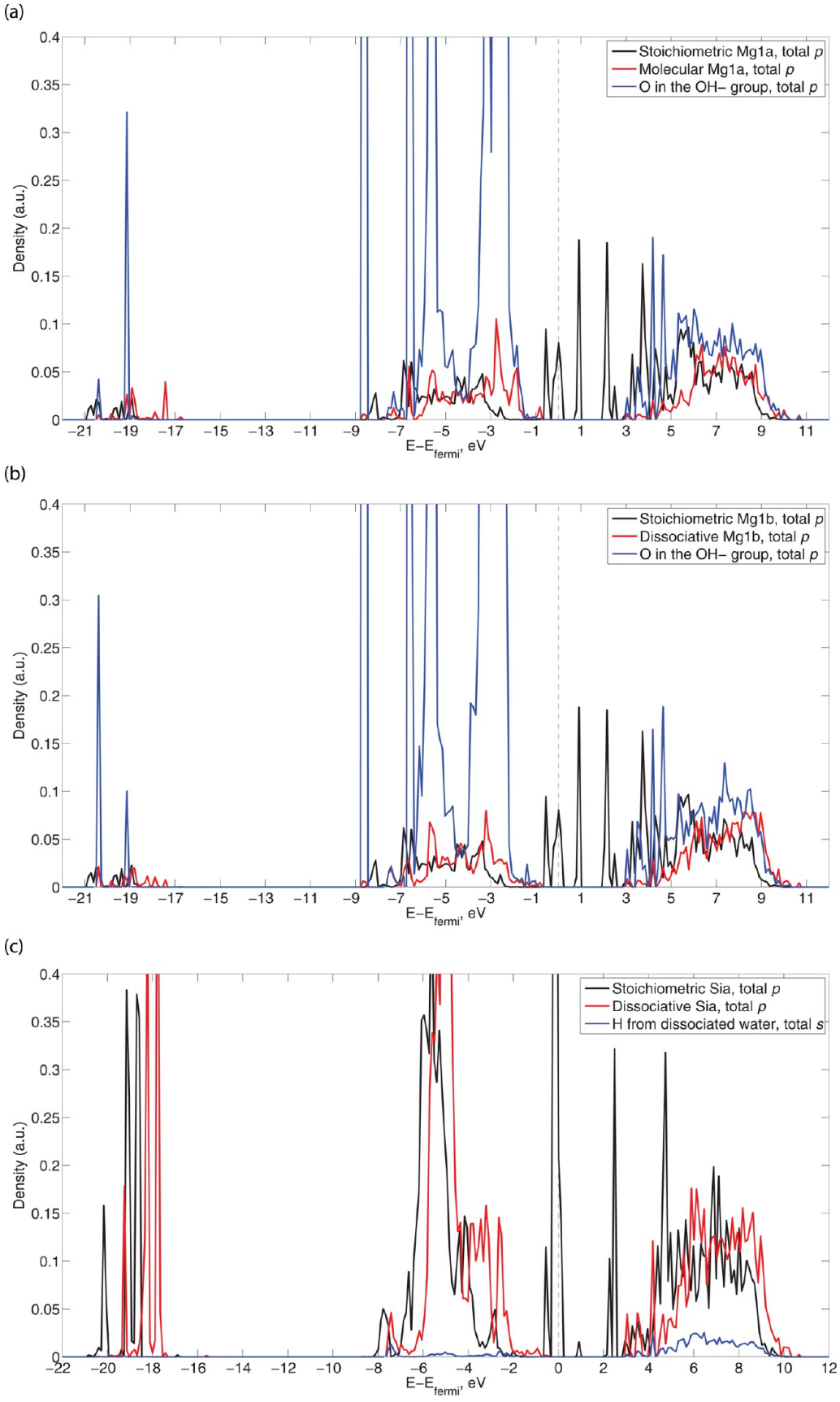

Figure 9. PDOS of the stoichiometric and hydrated Mg_2SiO_4 (100) surface. The hydrated Mg_2SiO_4 (100) termination is based upon mixed adsorption of two water molecules nearby the O2a and Mg1a surface sites. PDOS energies are referenced to the calculated Fermi level. Illustrated PDOS are (a) of the p orbital for Mg1a and oxygen atom in the OH group, (b) of the p orbital for Mg1b and oxygen atom in the OH group, and (c) of the p orbital for Sia and s orbital for the hydrogen atom.

dx.doi.org/10.1021/jp403271e | J. Phys. Chem. C 2013, 117, 21203−21216

the surface atoms in direct contact with H_2O or with H and OH groups upon dissociation.

From Table 3, it can be seen that water molecules, independent of the adsorption mechanism, gain charge upon interacting with the surface. The charge gained by the water molecule is close in value to the charge lost by the surface atoms. The small mismatch between the charge gained by the water and that lost by the surface could be due to the charge transfer from the top layer atoms to the atoms in the underlying layer, which has not been considered in this Bader charge analysis.

Projected Density of States (PDOS). The changes in the electronic structure upon adsorption of two water molecules at the O2a and Mg1a surface sites have been analyzed in this section.

The projected density of states (PDOS) of the stoichiometric and hydrated/hydroxylated surfaces of the interacting sites are shown in Figure 9. Here, the energies (E) of the orbitals are reported relative to the Fermi energy (E_{Fermi}) to illustrate the change in the properties of the surface after hydration. All of the sites involved in the formation of the hydrated surface groups, i.e., Mg1a, Mg1b, and Sia, have a nonzero PDOS at the Fermi level, as expected since they are all metal atoms. Above the Fermi level these surface sites show a broad energy band, indicating that they are reactive toward water, and in particular the Mg atom site as it presents high peaks close to the Fermi level. Upon interaction with water, the band gap widens up to 3 eV, suggesting that the sites upon interaction with water become insulating. It is known that the band gap of metal atoms is not estimated accurately by DFT; however, despite some small calculation error, the band gap change, here, is significant, and it can be associated with a physical phenomenon.[41] Moreover, the states in the valence band increase in energy as electrons move toward higher energy state, meaning that electrons are donated from the Mg atoms to the O atoms and from the Si atom to the H atom, which leads to a reduction in the Lewis acidity of these surface sites. This observation is also supported by the Bader charge analysis reported in the previous section. As a consequence of the electron donation, the width of the conduction band for all three surface sites decreases with the conduction band moving further from the Fermi level.

The clear overlap of the electronic states of Mg1a and Mg1b sites with the O atoms confirms the strong interaction between these atoms. Moreover, the changes in the PDOS at energies below the Fermi level suggest a covalent bonding interaction between the water molecules and a specific surface site which involves both s and p orbitals and to a larger extent of the latter over the former. Such a strong interaction may suggest that water molecules are chemisorbed onto the Mg_2SiO_4 surface as formulated earlier by de Leeuw et al.[42] and Stimpfl et al.[13] in their theoretical study reporting DFT calculations of water−forsterite interactions at low coverage.

Finally, the shift of the valence and conduction bands toward higher energy levels indicates that the surface becomes less stable upon hydration/hydroxylation as a consequence of the electron donation from the surface to the O and H atoms of the water molecules. The more significant overlap of the valence bands occurs at the Mg surface sites as a consequence of the Mg atoms more tightly bound to the O atoms of the water molecules, indicating a lower stability of these sites in comparison with the Si sites.

Effect of Coverage and Comparison with Calorimetric Measurements and Previous DFT Calculations. In this section, the effect of water coverage is analyzed and the calculated adsorption energies are compared with experimental data and previous DFT calculations. The experimental data are from calorimetric measurements performed by Chen and Navrotsky[16] at 25 °C and at saturated water pressures, while the DFT calculations were carried out by de Leeuw[12] and Stimpfl et al.[13] as reported in King et al.[14] Figure 10 shows all the adsorption energy data as a function of surface coverage θ.

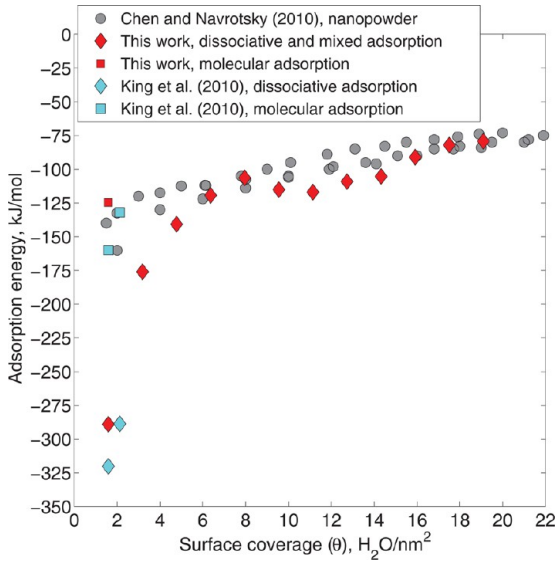

Figure 10. Adsorption energy (kJ/mol) as a function of the surface coverage (θ, H_2O/nm^2).

Chen and Navrotsky[16] calculate that one monolayer of water corresponds to approximately 10 H_2O/nm^2 and that there are about two monolayers of ordered water adsorbed onto the forsterite surface. Following their study, we considered in our calculations up to two monolayers of ordered water onto the Mg_2SiO_4 (100) surface with each monolayer comprising ~10 H_2O/nm^2.

At full monolayer coverage, Chen and Navrotsky[16] report an adsorption energy value of −100 kJ/mol of H_2O, while at two full monolayer coverage a value of −80 kJ/mol of H_2O. Our calculations show an adsorption energy approximately of −110.7 kJ/mol of H_2O at one monolayer coverage and −80 kJ/mol of H_2O for two monolayer coverage, which are in reasonable agreement with the experimental data. Below one monolayer coverage, our calculations predict that the most stable configuration corresponds to a hydrated Mg_2SiO_4 (100) termination where dissociative adsorption occurs thereby leading to adsorption energy values much lower than the one measured by Chen and Navrotsky.[16] However, at low coverage our calculations agree with previous DFT calculations for θ equal to 1.59 and 2.12 H_2O nm^2.

For the case of molecular adsorption, both our and previous DFT results compare well with the experimental data, suggesting that during the experiments equilibrium was not reached at low coverage and water did not dissociate but rather adsorbs molecularly.

Below 6 H_2O/nm^2 coverage, E_{ads} varies significantly, indicating a strong interaction between the water molecules and the forsterite surface, while above 6 H_2O/nm^2 coverage, the E_{ads} approaches a constant value of approximately −110.7 kJ mol^{-1}, suggesting that the interaction is much weaker and that the water molecules might be physisorbed. At higher

dx.doi.org/10.1021/jp403271e | J. Phys. Chem. C 2013, 117, 21203−21216

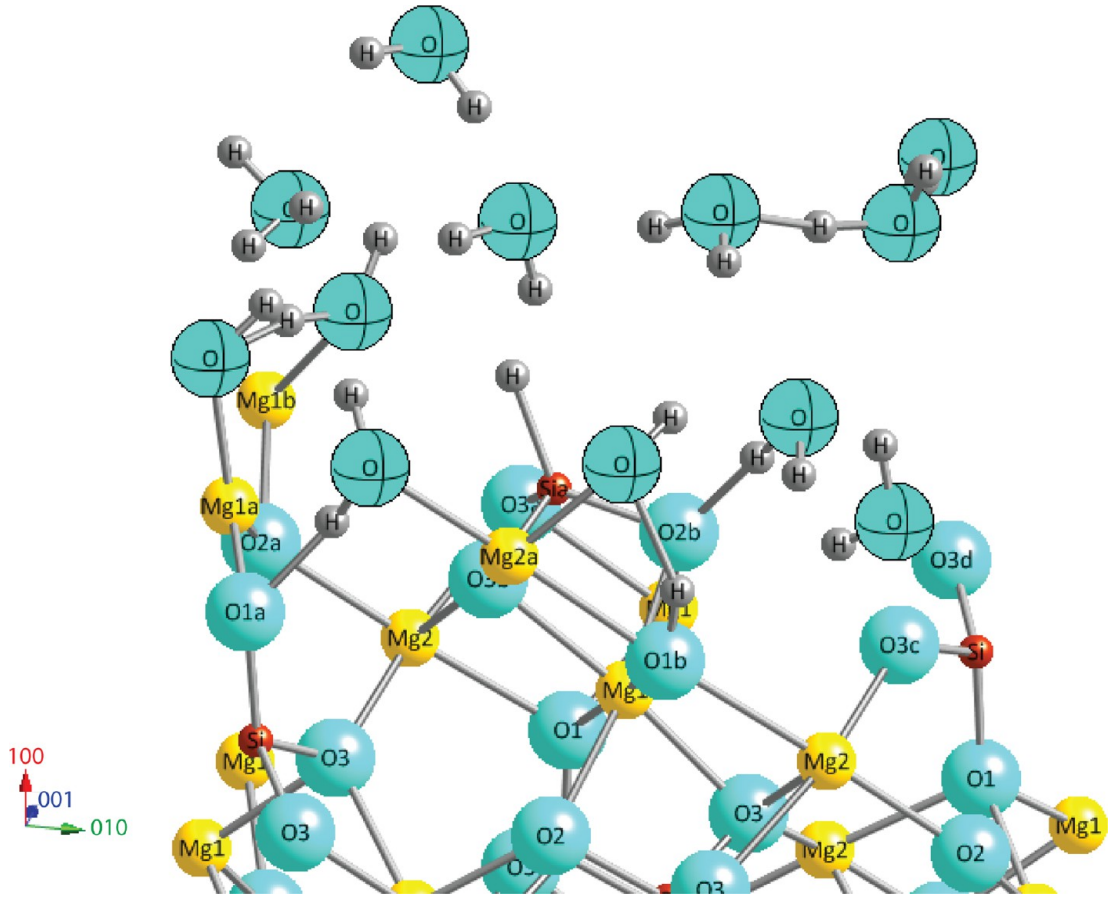

Figure 11. Two monolayers of water molecules on the Mg_2SiO_4 (100) surface. The oxygen atoms of the water molecules are highlighted with equatorial lines.

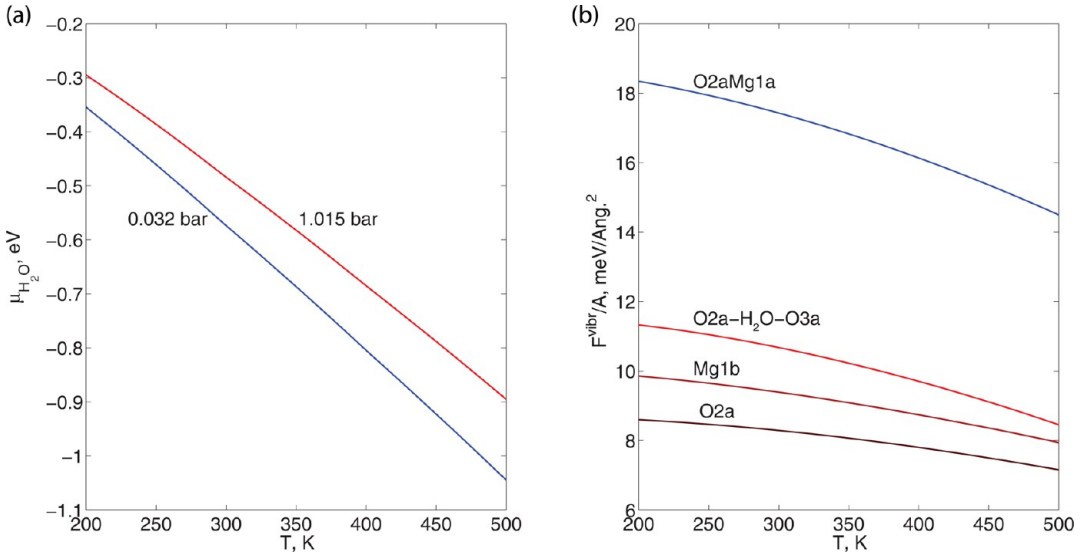

Figure 12. Contributions to the surface energy of the hydrated surface terminations as a function of temperature and P_{H_2O}: (a) chemical potential of gaseous water molecules (μ_{H_2O}); (b) vibrational energy (F^{vibr}) due to adsorbed water molecules.

coverage, molecular and dissociative adsorption occur and lead to the formation of a hydrogen-bonding network coordinating with the surface atoms. The formation of the hydrogen-bonding network for two monolayer coverages is shown in Figure 11. The first layer contains both dissociated and undissociated water molecules, while the second layer contains only molecularly adsorbed water.

Finally, we compared our values of the adsorption energy calculated for one and two monolayer coverage with those in the literature for water adsorbed on various mineral oxides. The values of E_{ads} are listed in Table 4. Here, it is possible to see that E_{ads} calculated in our work agrees well with all the literature values expect for α-quartz. The E_{ads} of SiO_2 is much smaller than E_{ads} of Mg_2SiO_4, indicating that the Mg_2SiO_4

dx.doi.org/10.1021/jp403271e | J. Phys. Chem. C 2013, 117, 21203−21216

Table 4. Comparison of the Adsorption Energy (kJ/mol of H_2O) of Mg_2SiO_4 (100) Surface with Literature Data from Theoretical and Experimental Work

	E_{ads} for one layer coverage (kJ/mol H_2O)	E_{ads} for two layer coverage (kJ/mol H_2O)
this work		
Mg_2SiO_4	−110.7	−80.0
experimental		
MgO[45]	−113	
CaO[44]	−145	
α-quartz[44]	−35	
DFT calculations		
MgO[43]	−3.9 to −175.9	
CaO[43]	−36.6 to −178.5	
α-quartz (0001)[46]	−40.0	
α-Al_2O_3 (0001)[47]		−106.1
β-MnO_2[48]	−94.6 to −129.3	

(100) surface becomes less stable than SiO_2 (0001) upon hydration.

CONCLUSION

In this paper, results based upon a theoretical approach to understand the interaction of forsterite with water are reported. They are determined from DFT electronic structure calculations in conjunction with *ab initio* thermodynamics and compared with earlier DFT calculations and available experimental data.

The calculations provide optimized surface structures and total energies at 0 K in vacuum for several configurations where H_2O interacts with the Mg_2SiO_4 (100) surface both via molecular and dissociative mechanisms. The average values of the calculated adsorption energies for a coverage of 1.59 H_2O/nm^2 range between −0.79 and −4.70 eV per water molecule, which is in agreement with previous literature data. While at increased coverages up to 20 H_2O/nm^2, i.e., two monolayers, the adsorption energy asymptotically approaches −0.82 eV per water molecule and agrees with the experimental data of calorimetric measurements.

Ab initio thermodynamics was used to extend the first-principles DFT calculations to atmospheric and hydrothermal conditions to provide predictions of the changes in surface stability as a function of temperature and pressure. Under the investigated conditions, the most stable configuration was identified with the interaction of two water molecules with the forsterite surface nearby O2 and Mg1 surface atoms. Upon interaction, one water molecule dissociates at the O2 site leading to the formation of an OH group and hydrogen binding to a Si atom, while the second water molecule molecularly adsorbs on the Mg1 site forming a hydronium group by reacting with the OH group from the first water molecule. Significant surface reconstruction is observed with the elongation of the Mg−O surface bonds. Bader charge and density of state analyses indicate that significant charge is lost from the surface atoms toward the water molecule groups, suggesting that water is chemisorbed at the Mg surface atoms resulting in decreased stability compared to the Si atom.

APPENDIX. CHEMICAL POTENTIAL AND VIBRATIONAL ENERGY

Figure 12 illustrates the contribution of the chemical potential of water (μ_{H_2O}) and vibrational energy (F^{vibr}) change with temperature and pressure. The contribution of μ_{H_2O} decreases with temperature and increases with P_{H_2O}, as expected, while the contribution of F^{vibr} decreases with temperature and type of hydrated terminations. The vibrational frequencies ω_k in eq 6 were calculated allowing only the hydrogen atoms and the OH groups to vibrate as the vibrational contribution is the most significant for light atoms and light groups.

AUTHOR INFORMATION

Corresponding Author

*E-mail: valentina.prigiobbe@austin.utexas.edu; Ph +1 (512) 232-2481; Fax +1 (512) 471-9605 (V.P.).

Notes

The authors declare no competing financial interest.

ACKNOWLEDGMENTS

Work at the University of Austin was supported by the Center for Frontiers of Subsurface Energy Security (CFSES), an Energy Frontier Research Center funded by DOE, Office of Science, BES under Award DE-SC0001114. This work used the Extreme Science and Engineering Discovery Environment (XSEDE), which is supported by National Science Foundation Grant OCI-1053575. The computational resources were by the Texas Advanced Computing Center (TACC) and partially by the Stanford Center for Computational Earth and Environmental Science (CEES). We thank Dr. Dong-Hee Lim for his valuable support in the VASP simulations during the early phase of this project.

REFERENCES

(1) *IPCC Special Report on Carbon Dioxide Capture and Storage*; Technical Report; Cambridge University Press: Cambridge, UK, 2005.
(2) Seyama, H.; M, S.; Tanaka, A. *Chem. Geol.* **1988**, *129*, 209−216.
(3) Wogelius, R.; Walther, J. *Geochim. Cosmochim. Acta* **1991**, *55*, 943−954.
(4) Awad, A.; van Groos, A.; Guggenheim, S. *Geochim. Cosmochim. Acta* **2000**, *64*, 1765−1772.
(5) Pokrovsky, O.; Schott, J. *Geochim. Cosmochim. Acta* **2000**, *64*, 3299−3312.
(6) Rosso, J. J.; Rimstidt, J. D. *Geochim. Cosmochim. Acta* **2000**, *64*, 797−811.
(7) Hänchen, M.; Prigiobbe, V.; Storti, G.; Seward, T. M.; Mazzotti, M. *Geochim. Cosmochim. Acta* **2006**, *70*, 4403−4416.
(8) Zakaznova-Herzog, V.; Nesbitt, H.; Bancroft, G.; Tse, J.; Gao, X.; Skinner, W. *Phys. Rev. B* **2005**, *72*, 205113.
(9) Prigiobbe, V.; Costa, G.; Baciocchi, R.; Hänchen, M.; Mazzotti, M. *Chem. Eng. Sci.* **2009**, *64*, 3510−3515.
(10) Oelkers, E. H.; Golubev, S. V.; Chairat, C.; Pokrovsky, O. S.; Schott, J. *Geochim. Cosmochim. Acta* **2009**, *73*, 4617−4634.
(11) Prigiobbe, V.; Mazzotti, M. *Chem. Eng. Sci.* **2011**, *66*, 6544−6554.
(12) de Leeuw, N. *J. Phys. Chem. B* **2001**, *105*, 9747−9754.
(13) Stimpfl, M.; Walker, A.; Drake, M.; de Leeuw, N.; Deymier, P. *J. Cryst. Growth* **2006**, *294*, 83−95.
(14) King, H.; Stimpfl, M.; Deymier, P.; Drake, M.; Catlow, C.; Putnis, A.; de Leeuw, N. *Earth Planet. Sci. Lett.* **2010**, *300*, 11−18.
(15) Watson, G. W.; Oliver, P. M.; Parker, S. C. *Phys. Chem. Miner.* **1997**, *25*, 70−78.
(16) Chen, S.; Navrotsky, A. *Am. Mineral.* **2010**, *95*, 112−117.
(17) Loring, J. S.; Thompson, C. J.; Wang, Z.; Joly, A. G.; Sklarew, D. S.; Schaef, H. T.; Ilton, E. S.; Rosso, K. M.; Felmy, A. R. *Environ. Sci. Technol.* **2011**, *45*, 6204−6210.
(18) Kerisit, S.; Weare, J. H.; Felmy, A. R. *Geochim. Cosmochim. Acta* **2012**, *84*, 137−151.
(19) Catalano, J. G.; Park, C.; Zhang, Z.; Fenter, P. *Langmuir* **2006**, *22*, 4668−4673.

(20) Catalano, J. G.; Fenter, P.; Park, C. *Geochim. Cosmochim. Acta* **2007**, *71*, 5313−5324.
(21) Aboud, S.; Wilcox, J.; Brown, G. E. *Phys. Rev. B* **2011**, *83*, 125407.
(22) Lo, C. S.; Tanwar, K. S.; Chaka, A. M.; Trainor, T. P. *Phys. Rev. B* **2007**, *75*, 075425.
(23) Birle, J. D.; Gibbs, G. V.; Moore, P. B.; Smith, J. V. *Am. Mineral.* **1968**, *53*, 807−824.
(24) Chatterjee, S.; Bhattacharyya, S.; Sengupta, S.; Saha-Dasgupta, T. *Phys. Chem. Miner.* **2011**, *38*, 259−265.
(25) Kresse, G.; Furthmuller, J. *Comput. Mater. Sci.* **1996**, *6*, 15−50.
(26) Perdew, J.; Burke, K.; Ernzerhof, M. *Phys. Rev. Lett.* **1996**, *77*, 3865−3868.
(27) Blochl, P. *Phys. Rev. B* **1994**, *50*, 17953−17979.
(28) Kresse, G.; Joubert, D. *Phys. Rev. B* **1999**, *59*, 1758−1775.
(29) Monkhorst, H.; Pack, J. *Phys. Rev. B* **1976**, *13*, 5188−5192.
(30) Smyth, J.; Hazen, R. *Am. Mineral.* **1973**, *58*, 588−593.
(31) Kudoh, Y.; Takeuchi, Y. *Z. Kristallogr.* **1985**, *171*, 291−302.
(32) Brodholt, J. *Am. Mineral.* **1997**, *82*, 1049−1053.
(33) *CRC Handbook of Chemistry and Physics*, 92nd ed.; CRC: Boca Raton, FL, 2012.
(34) Rogal, J.; Reuter, K. Educational Notes, RTO-EN-AVT-142, 2007.
(35) Sun, Q.; Reuter, K.; Scheffler, M. *Phys. Rev. B* **2003**, *67*, 205424.
(36) NIST-JANAF Thermochemical Tables. Table of Gasous Water; Technical Report.
(37) Kudoh, Y.; Kuribayashi, T.; Kagi, H.; Inoue, T. *J. Miner. Petrol. Sci.* **2006**, *101*, 265−269.
(38) Liu, Y.; Olsen, A.; Rimstidt, J. *Am. Mineral.* **2006**, *91*, 455−458.
(39) Kwak, J. H.; Hu, J. Z.; Hoyt, D. W.; Sears, J. A.; Wang, C.; Rosso, K. M.; Felmy, A. R. *J. Phys. Chem. C* **2010**, *114*, 4126−4134.
(40) Sanville, E.; Kenny, S. D.; Smith, R.; Henkelman, G. *J. Comput. Chem.* **2007**, *28*, 899−908.
(41) Sholl, D. S.; Steckel, J. A. *Density Functional Theory*; Wiley: Hoboken, NJ, 2009.
(42) de Leeuw, N.; Parker, S.; Catlow, C.; Price, G. *Phys. Chem. Miner.* **2000**, *27*, 332−341.
(43) de Leeuw, N.; Watson, G.; Parker, S. *J. Phys. Chem.* **1995**, *99*, 17219−17225.
(44) Fubini, B.; Bolis, V.; Bailes, M.; Stone, F. S. *Solid State Ionics* **1989**, *32/33*, 258−272.
(45) Beruto, D.; Searcy, A.; Botter, R.; Giordani, M. *J. Phys. Chem.* **1993**, *97*, 9201−9205.
(46) Du, Z.; de Leeuw, N. *Surf. Sci.* **2004**, *554*, 193−210.
(47) Ranea, V. A.; Schneider, W. F.; Carmichael, I. *Surf. Sci.* **2008**, *602*, 268−275.
(48) Oxford, G. A. E.; Chaka, A. M. *J. Phys. Chem. C* **2012**, *116*, 11589−11605.